

## A SPECTROPHOTOMETRIC SEARCH FOR GALAXY CLUSTERS IN SDSS

JOO H. YOON,<sup>1,2</sup> KEVIN SCHAWINSKI,<sup>3</sup> YUN-KYEONG SHEEN,<sup>1,2</sup> CHANG H. REE,<sup>4</sup> AND SUKYOUING K. YI<sup>1,2</sup>

Received 2007 June 13; accepted 2007 December 3

### ABSTRACT

Recent large-scale galaxy spectroscopic surveys, such as the Sloan Digital Sky Survey (SDSS), enable us to execute a systematic, relatively unbiased search for galaxy clusters. Such surveys make it possible to measure the 3D distribution of galaxies but are hampered by the incompleteness problem due to fiber collisions. In this study we aim to develop a density-measuring technique that alleviates the problem and derives densities more accurately by adding additional cluster member galaxies that follow optical color-magnitude relations for the given redshift. The new density measured with both spectroscopic and photometric data shows a good agreement with apparent information on cluster images and is supported by follow-up observations. By adopting this new method, a total of 924 *robust* galaxy clusters are found from the SDSS DR5 database in the redshift range  $0.05 < z < 0.1$ , of which 212 are new. Local maximum-density galaxies successfully represent cluster centers. We provide the cluster catalog including a number of cluster parameters.

*Subject headings:* catalogs — galaxies: clusters: general — galaxies: general — surveys

*Online material:* color figures, machine-readable table

### 1. INTRODUCTION

The role of environment in the formation and evolution of galaxies is a topic of much interest in modern astrophysics. Dressler (1980) found that the abundance of early-type galaxies increases in dense environment, indicating that environment has an effect on galaxy morphology. This *morphology-density relation* has been further studied by many authors (e.g., Whitmore & Gilmore 1991; Dressler et al. 1997; Goto et al. 2003; Capak et al. 2007; Park et al. 2007) and has been extended to lower density regions and high-redshift clusters (Postman & Geller 1984; Giovanelli et al. 1986; Tully 1988). There have been several physical mechanisms proposed to explain this relation, such as ram pressure stripping (Gunn & Gott 1972; Farouki & Shapiro 1980; Fujita & Nagashima 1999; Abadi et al. 1999; Quilis et al. 2000; Chung et al. 2007), tidal forces (Byrd & Valtonen 1990; Valluri 1993), galaxy harassment (Moore et al. 1996, 1999), starvation (Larson et al. 1980), and interaction and merging (Toomre & Toomre 1972; Makino & Hut 1997; Bekki 1999; Boselli & Gavazzi 2006; Chung et al. 2007).

Some of these processes involve violent gas dynamics, and hence it is quite likely that environment influences the star formation rate in galaxies (Gisler 1978; Larson & Tinsley 1978; Lewis et al. 2002; Gomez et al. 2003; Christlein & Zabludoff 2005; Elbaz et al. 2007). The cosmic star formation history itself is also suspected to depend on environment (Thomas et al. 2005). Perhaps as hints of these suspicions, galaxy properties such as color, luminosity, and size appear to depend on environment (Balogh et al. 2004a, 2004b; Blanton et al. 2005; Croton et al. 2005; Postman et al. 2005; Quintero et al. 2006; Park et al. 2007). However, the exact physical processes that link between galaxy properties and environment are still far from being clear.

Galaxy clusters are the most dense regions in the large-scale universe. The number density of galaxies in clusters can be several hundred times larger than that of the field. They are thus ideal laboratories for studying the effect of environment on the formation and evolution of galaxies.

The first galaxy cluster catalogs (Abell 1958; Zwicky et al. 1961–1968; Abell et al. 1989) were based on the visual inspection of photographic plates. While these catalogs have been widely adopted, they suffer from many selection effects and spurious detections due to projection effects. Furthermore, the visual inspection of large parts of the sky is very time consuming. Systematic searchers for galaxy clusters are needed to ensure the efficiency and reliability of the cluster detection. Among the most popular in the absence of spectroscopic information were the technique using the early-type galaxy color-magnitude relation (Gladders & Yee 2000) and finding brightest cluster galaxies (BCGs; Bahcall et al. 2003; von der Linden et al. 2007). The first automatic search for optical clusters looking for overdense regions was by Shectman (1985) followed by numerous others (Lumsden et al. 1992; Dalton et al. 1994; Postman et al. 1996; Croft et al. 1997; Kim et al. 2002; Kochanek et al. 2003; Miller et al. 2005).

With the advent of large-area, spectroscopic redshift surveys, such as the Sloan Digital Sky Survey (SDSS; York et al. 2000; Stoughton et al. 2002) and Two Degree Field Galaxy Redshift Survey (2dFGRS; Colless et al. 2001), large cosmological volumes with redshift have become available. We are finally able to systematically search for galaxy clusters in a large volume by measuring the local 3D number density of galaxies. While the 3D densities measured based on the spectroscopic database are more powerful than projection-based 2D searches for delineating the local galaxy distribution, they require a high level of coverage of member galaxies in the spectroscopic survey a priori. However, even the most up-to-date surveys (such as the SDSS) show only ~60%–70% completeness rate in dense regions, hampering us from measuring the densities accurately. In this paper, we introduce an improved method for finding galaxy clusters by measuring local densities using both spectroscopic and *photometric* data and provide a new catalog of the clusters that we have found. We assume cosmological parameters  $\Omega_m = 0.3$ ,  $\Omega_\Lambda = 0.7$ ,  $q_0 = -0.55$ , and  $H_0 = 70 \text{ km s}^{-1} \text{ Mpc}^{-1}$  throughout this paper, and all distances are comoving.

### 2. THE DATA

The SDSS is performing a survey to cover one-quarter of the whole sky. The imaging survey of the SDSS DR5 contains 215 million objects in  $8000 \text{ deg}^2$ . The SDSS spectroscopic survey

<sup>1</sup> Department of Astronomy, Yonsei University, Seoul 120-749, Korea; yi@yonsei.ac.kr.

<sup>2</sup> Center for Space Astrophysics, Yonsei University, Seoul 120-749, Korea.

<sup>3</sup> Department of Physics, University of Oxford, Oxford OX1 3RH, UK.

<sup>4</sup> Korea Astronomy and Space Science Institute, 61-1 Hwaam-dong, Yuseong-gu, Daejeon 305-348, Korea.

mapped 5740 deg<sup>2</sup>, obtaining about 1 million spectra of which 674,749 objects are classified as galaxies. The galaxy redshifts provided make it possible to study the 3D structure of galaxy distribution.

The SDSS photometric pipeline provides several kinds of magnitudes. For galaxy colors, we use the modelMags, as they provide unbiased colors regardless of any color gradients. For galaxy luminosities, we use petroMags, as these are a better estimate of the total luminosity (Stoughton et al. 2002). We also apply a  $K$ -correction as described in Blanton et al. (2003b) and correct for Galactic extinction with the Schlegel et al. (1998) values provided by the SDSS pipeline.

We use the SDSS DR5 both photometric and spectroscopic data. For the galaxies with spectra, we extract *all types of galaxies* in the range  $0.05 < z < 0.1$  and having  $r_{\text{petro}} < 17.77$  (Strauss et al. 2002). At  $z = 0.1$ ,  $r = 17.77$  corresponds to an absolute magnitude of  $M_r = -20.55$ . In order to create a volume-limited sample and so avoid biases with redshift, we cut at this absolute magnitude.

For galaxies without spectra, we select all galaxies with  $13.00 < r_{\text{petro}} < 17.77$  to have the same apparent magnitude cut as the spectroscopic data. Its faint limit comes from the SDSS spectroscopic survey limit, and the bright limit is from the fact that the objects of  $r_{\text{petro}} < 13.00$  and  $z > 0.05$  are almost always stars rather than galaxies.

### 3. MEASURING GALAXY DENSITY

#### 3.1. Local Density Measurement

Popular methods to measure galaxy local densities include a simple estimation of spatial number density in a certain radius and the distance to the  $n$ th nearest galaxy. The number density, however, cannot tell us about the concentration status, which is critical for studying dynamical evolution, while using the  $n$ th nearest galaxy can be biased by local density fluctuations. Thus, in addition to the number density, the spatial separation between galaxies can be taken into account as well to provide additional information. For example, closer neighbors can be weighted more than distant galaxies. Schawinski et al. (2007, hereafter S07) introduced such a weighting scheme with a Gaussian filter. The S07 scheme considers neighboring galaxies in the ellipsoid defined by

$$\left(\frac{r_a}{3\sigma}\right)^2 + \left(\frac{r_z}{3c_z\sigma}\right)^2 \leq 1, \quad (1)$$

where  $\sigma$  is the searching distance criterion,  $r_a$  is the projected distance, and  $r_z$  is the line-of-sight distance, all in Mpc, to a neighboring galaxy. It allows all the galaxies within the ellipsoid to be counted for measuring the density. The  $c_z$  factor is a simple compensation for the ‘‘finger-of-God’’ effect due to the peculiar motion and is estimated by counting the number of galaxies  $n$  within the sphere of radius  $\sigma$  as

$$c_z = 1 + 0.2n, \quad (2)$$

where  $n$  is capped at 10. Hence, this can scale along the radial direction up to a factor of 3. Density measures by adopting a fixed volume in comoving space can lead to sampling vastly different volumes in the field and in clusters due to the stretching of the line-of-sight direction by the finger-of-God effect.

The density parameter to each member galaxy based on the spectroscopic data is calculated as

$$\rho_{\text{spec,3D}}(\sigma) = \frac{1}{\sqrt{2\pi}\sigma} \sum_i \exp\left[-\frac{1}{2}\left(\frac{r_{a,i}^2}{\sigma^2} + \frac{r_{z,i}^2}{c_z^2\sigma^2}\right)\right] \quad (3)$$

by summing up for all the members within the search ellipsoid. The target galaxy is not included in the density summation. Our algorithm estimates the local density with surrounding galaxies in a relatively large area and thus minimizes local effects.

In this paper, we attempt to improve the density measurement scheme of S07 by adding photometric member candidates and build on the S07 algorithm to design an effective cluster search method.

#### 3.2. Member Selection with Spectroscopic Data

Since we do not have the line-of-sight information on the photometric member galaxies, we first measure the 2D densities for our spectroscopic galaxy samples ignoring the line-of-sight information.

We first define an ellipsoid as in S07:

$$\left(\frac{r_a}{\sigma_1}\right)^2 + \left(\frac{r_z}{\sigma_2}\right)^2 \leq 1. \quad (4)$$

We choose  $\sigma_1 = 1$  Mpc because it optimizes the search for the density peak and the brightest cluster galaxy of the cluster. For  $\sigma_2$  we adopt the distance corresponding to 3 times the velocity dispersion of the cluster. Note that  $\sigma_2$  is used only for selecting member galaxies but not for the 2D density measurement. Readers are referred to § 3.5 for more details. Galaxies within the ellipsoid are regarded as member galaxies of the cluster. Then the new 2D density  $\rho_{\text{spec}}$  for the spectroscopic members is

$$\rho_{\text{spec}} = \frac{1}{\sqrt{2\pi}\sigma_1} \sum_i \exp\left[-\frac{1}{2}\left(\frac{r_{a,i}^2}{\sigma_1^2}\right)\right], \quad (5)$$

where  $\sigma_1 = 1$  Mpc.

#### 3.3. Member Selection with Photometric Data

The SDSS spectroscopic survey tries to cover galaxies as completely as possible with a tiling algorithm (Blanton et al. 2003a). However, its selection scheme can leave some galaxies unobserved due to fiber collisions. Figure 1 shows the extreme case of Abell 2670, which shows only 65% of spectroscopic coverage rate within the 1 Mpc radius from the cluster center. This effect is generally worse for denser regions because the fiber collision problem is obviously worse in the more crowded regions. We estimate the spectroscopic completeness, that is, the number fraction of galaxies covered by the SDSS DR5 spectroscopic survey, to be  $f_{\text{spec}} \sim 65\%$  for rich clusters. An independent study has also reported that 30% of true brightest cluster galaxies are missed by the spectroscopic survey (von der Linden et al. 2007). The ‘‘incompleteness’’ of the spectroscopic survey causes a problem in measuring the densities of galaxies in dense regions. We attempt to alleviate this by further considering photometric data.

Early-type galaxies in clusters have a tight correlation between their optical colors and luminosity, known as the color-magnitude relation (CMR). The CMR was first observed by Baum (1959) and is often reported to be universal within errors (Visvanathan & Sandage 1977; Hogg et al. 2004; López-Cruz et al. 2004). Based on these assumptions, we can select candidate cluster members even though they do not have redshift because galaxies on the CMR have a high likelihood of belonging to the cluster. Thus, we find the slope and scatter of the CMR in order to select ‘‘photometric members.’’ For small clusters, the slope of the CMR can be difficult to achieve. Hence, we construct an empirical CMR by stacking galaxies that are members of 20 typical

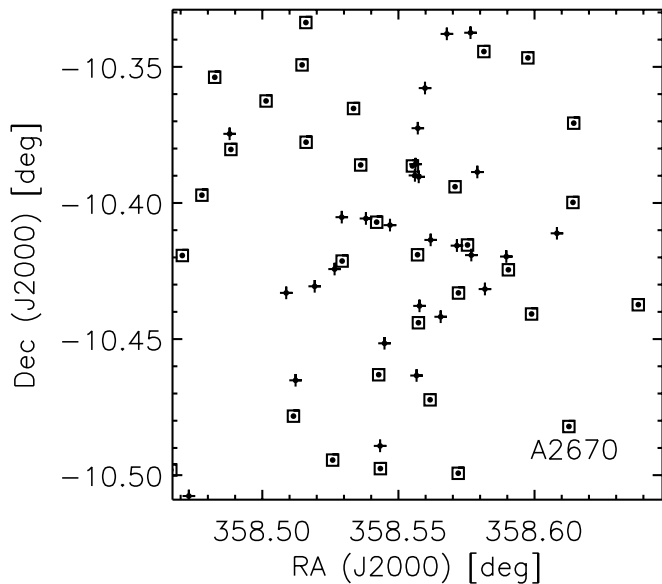


FIG. 1.—Spectroscopic completeness for the case of Abell 2670 with  $r_{\text{petro}} < 17.77$ . The dots with rectangles are galaxies covered by the SDSS spectroscopic survey, and the crosses are the missed ones. The completeness rate for this cluster is only 55% in this field of view and 65% within 1 Mpc radius from the cluster center. This figure illustrates the problem of fiber collisions in dense environments. [See the electronic edition of the Supplement for a color version of this figure.]

clusters determined by their redshifts. We do this for five redshift bins with  $\Delta z = 0.01$ , and an example is shown in Figure 2. A linear fit with  $2\sigma$  clipping is iterated until the number of galaxies on the CMR remains constant. The galaxies residing on the CMR  $\pm 3\text{rms}$  in  $g-r$  color are selected as photometric members. We compute the 2D photometric density  $\rho_{\text{phot}}$  following equation (5) using only the photometric members.

The total density  $\rho$  of a galaxy is calculated by combining the spectroscopic and photometric density parameters:

$$\rho = \rho_{\text{spec}} + \rho_{\text{phot}}. \quad (6)$$

In the process of combining  $\rho_{\text{spec}}$  and  $\rho_{\text{phot}}$  we are losing the line-of-sight information and our density measures are projected into only two dimensions; however, our method still provides improved density measures as is demonstrated in § 4 through our follow-up spectroscopic observations.

When we determine whether a particular galaxy without redshift belongs to a cluster as described in this section, we assume that the galaxy is at the redshift of the cluster and apply the same absolute magnitude cut as discussed in § 2.

We have attempted to improve our local density measure further by applying a galaxy luminosity weight (i.e., weighting more luminous galaxies more) but found no significant difference. Hence, we have decided to ignore it.

### 3.4. The Efficiency of the CMR Technique

We expect the CMR to be effective for finding cluster member galaxies but that it may still suffer from the projection effect of background and foreground objects. Hence, we test its efficiency. We restrict the test to the spectroscopic data only, because only with redshift can we determine whether a particular galaxy is a cluster member or not, that is, for a convincingly high confidence. Besides, we use early-type galaxies (ETGs) alone for this test, as our CMR method works only for them. In order to select ETGs, we use the morphological index  $\text{fracDev}$  from the SDSS pipeline, which shows the weight of the de Vaucouleurs

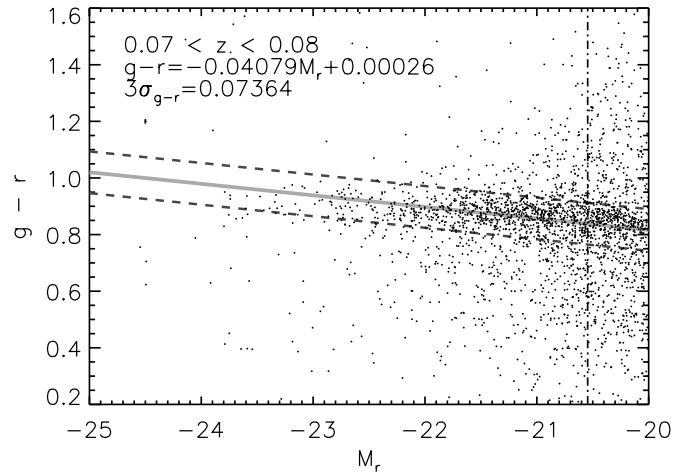


FIG. 2.—Empirical CMR for the redshift range  $0.07 < z < 0.08$ . The gray solid line shows a linear fit after  $2\sigma$  clipping until the number of galaxies on the CMR becomes constant, and the dashed lines show the scatter (the gray solid line  $\pm 3\sigma$  in  $g-r$  color). The vertical dot-dashed line is an absolute magnitude cut in our data selection. [See the electronic edition of the Supplement for a color version of this figure.]

profile in the two-component profile fit with the de Vaucouleurs and exponential profiles. We apply the highly conservative  $r$ -band  $\text{fracDev} > 0.95$  cut, and the galaxies selected are highly likely to be early type. Using the spectroscopic members meeting the same  $\text{fracDev}$  criterion, we check the validity of our scheme defining the following two CMR-related quantities.

$$\text{Completeness} = \frac{\text{No. of ETG members in CMR}}{\text{No. of all ETG cluster members}} \times 100, \quad (7)$$

$$\text{Purity} = \frac{\text{No. of ETG members in CMR}}{\text{No. of ETG galaxies in CMR}} \times 100. \quad (8)$$

The “CMR completeness” is a measure of the number of early-type cluster members that also sit on the CMR. The “CMR purity” tells us the fraction of galaxies selected by the CMR method that are indeed early-type cluster members. Figure 3

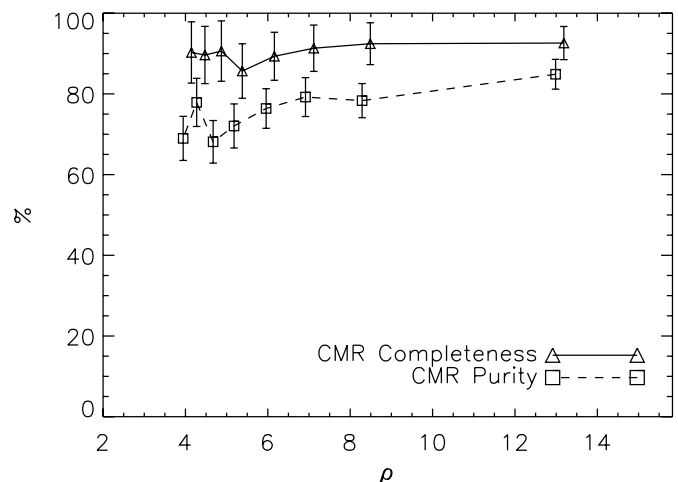


FIG. 3.—Solid and dashed lines show completeness and purity, respectively, of the photometric member candidates found from our technique (see text for definition). The errors are from the Poisson statistics in the equal number bin. The rectangles are shifted slightly to the left for the clarity of the figure. The completeness is constantly  $\sim 90\%$  and the purity is 70%–85% with an apparent density dependence. The high values of these parameters validate our CMR technique.

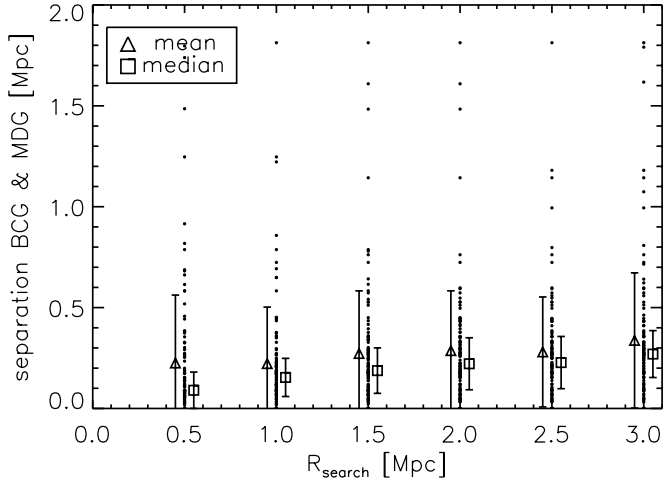


FIG. 4.—Projected separation between brightest cluster galaxies (BCGs) and maximum-density galaxies (MDGs). Triangles denote the mean and squares the median separations. The error bars show the standard deviation for the mean and the median absolute deviation for the median. When the search radius to find member galaxies is 1 Mpc, the separation is small enough that the cluster search is effective. But a substantially smaller value than 1 Mpc would miss many member galaxies because the typical size of clusters can be easily as large as 1 Mpc (see text). [See the electronic edition of the Supplement for a color version of this figure.]

presents the CMR completeness and purity of our clusters as a function of density. The CMR completeness is around 90%, meaning that 90% of the early-type (by fracDev) member galaxies indeed sit on the CMR. The purity is 70%–85%, meaning that only 70%–85% of the galaxies on the CMR are early-type (by fracDev) members. The rest may be background or foreground galaxies. Exact values of these parameters modestly depend on the fracDev criterion adopted, but on the whole both parameters show high values, validating our scheme.

### 3.5. Finding Clusters

The SDSS DR5 photometric data include about 1 million galaxies in the magnitude range described in § 2. Searching for clusters through the entire data set would require an exhaustive amount of effort. So we begin our cluster search first by estimating the local density of *spectroscopic* members and identify about

7000 galaxies with high density measures as candidate cluster positions. For this selection we use a 3D spectroscopic density parameter ( $\rho_{\text{spec,3D}} > 0.5$ ).

We then select all the photometric and spectroscopic galaxies within a 2 Mpc radius from the cluster center candidate galaxies and estimate their total 2D local density with both the spectroscopic and photometric members for all galaxies in this radius.

With these 2D spectrophotometric density measurements, we find the galaxy with the highest density in the area of a 2 Mpc circle and  $\Delta z = 0.01$ . The highest density galaxy in a local area is defined as the maximum-density galaxy (MDG). As the MDG resides at the densest part of the selected volume, we define it as the cluster center and declare it a cluster if the  $\rho$  of an MDG is greater than 4.0, which roughly corresponds to a cluster velocity dispersion of 200 km s<sup>-1</sup>.

We expect that the MDG should be close to the cluster center and coincide with the brightest cluster galaxy (Matthews et al. 1964; Oegerle & Hill 2001). We compared the projected separation of BCGs to MDGs and found that they do not always coincide, however. We assume that a good cluster search scheme should identify MDGs as BCGs as well, and thus we vary the member search radius (the short axis of the ellipsoid) hoping to minimize the separation.

Figure 4 shows the separation between MDGs and BCGs. The mean and error bars reflect the large scatter in the sample. The median is a better estimate of the typical distance and shows a convergence toward a lower value of search radius. However, too small a value of the search radius would miss too many member galaxies in the density measurement and be dominated by local density fluctuations. The typical virial radius of our clusters is 0.5 Mpc in the 2D projection, and a substantial fraction (~50%) of clusters have a virial radius greater than 0.5 Mpc and extend beyond 1 Mpc. Considering this, we have chosen 1 Mpc as our search radius. It should be noted that our search using spectroscopic data and the CMR is liable to missing clusters that are dominated by blue, star-forming galaxies, if any.

## 4. RESULTS

### 4.1. Cluster Catalog and Properties

We provide our cluster catalog in Table 1. We have found 924 galaxy cluster candidates with  $\rho \geq 4.0$ , which roughly corresponds

TABLE 1  
CLUSTER CATALOG WITH  $\rho \geq 4$

ID	RA <sub>MDG</sub> (J2000.0)	Dec <sub>MDG</sub> (J2000.0)	$z_{\text{clt}}$	$\rho$	$N_{200}$	$R_{200}$	$\sigma_v$	RA <sub>BCG</sub> (J2000.0)	Dec <sub>BCG</sub> (J2000.0)	$z_{\text{BCG}}$	Comments
(1)	(deg)	(deg)	(4)	(5)	(6)	(Mpc)	(km s <sup>-1</sup> )	(deg)	(deg)	(11)	(12)
1.....	258.20851	64.05295	0.08257	32.197	148	2.785	1299	258.12006	64.06076	0.07340	A2255
2.....	358.55746	-10.39042	0.07623	29.234	91	1.842	840	358.55703	-10.41904	0.07766	A2670
3.....	208.26551	5.13824	0.07945	25.020	50	1.421	780	208.27667	5.14974	0.07890	A1809
4.....	228.81884	4.37958	0.09796	24.611	65	1.487	864	228.80879	4.38621	0.00000	A 2048
5.....	255.66908	33.52032	0.08819	22.783	74	1.813	1135	255.63809	33.51666	0.08640	A2245
6.....	239.58334	27.23342	0.08969	22.476	190	2.918	1000	239.58334	27.23342	0.09081	A2142
7.....	205.54886	2.22449	0.07688	21.140	41	1.286	845	205.54018	2.22721	0.00000	A1773
8.....	186.91015	8.82133	0.08981	20.599	41	1.305	849	186.87809	8.82456	0.00000	A1541
9.....	230.33576	30.67093	0.07845	19.313	76	1.723	677	230.33576	30.67093	0.07845	A 2061
10.....	255.64172	34.07809	0.09871	19.178	64	1.546	1120	255.67708	34.06003	0.09891	A2244

NOTES.—Col. (1): ID; cols. (2) and (3): the coordinates of the maximum-density galaxies (MDGs); col. (4): the redshift of clusters estimated with spectroscopic data; col. (5): the density of the cluster MDG within 1 Mpc; col. (6): the number of member galaxies of clusters within  $R_{200}$ ; col. (7): the virial radius of clusters obtained by the number density profile of the galaxy clusters; col. (8): the velocity dispersion within  $R_{200}$ ; cols. (9) and (10): the coordinates of the brightest cluster galaxies; col. (11): the redshift of the BCGs (entries with zero mean the absence of the redshift information); col. (12): matching result with known catalog of galaxy clusters. The complete version of the galaxy clusters is available on the Web page <http://gem.yonsei.ac.kr/html/cluster.php>. Table 1 is published in its entirety in the electronic edition of the *Astrophysical Journal Supplement*. A portion is shown here for guidance regarding its form and content.

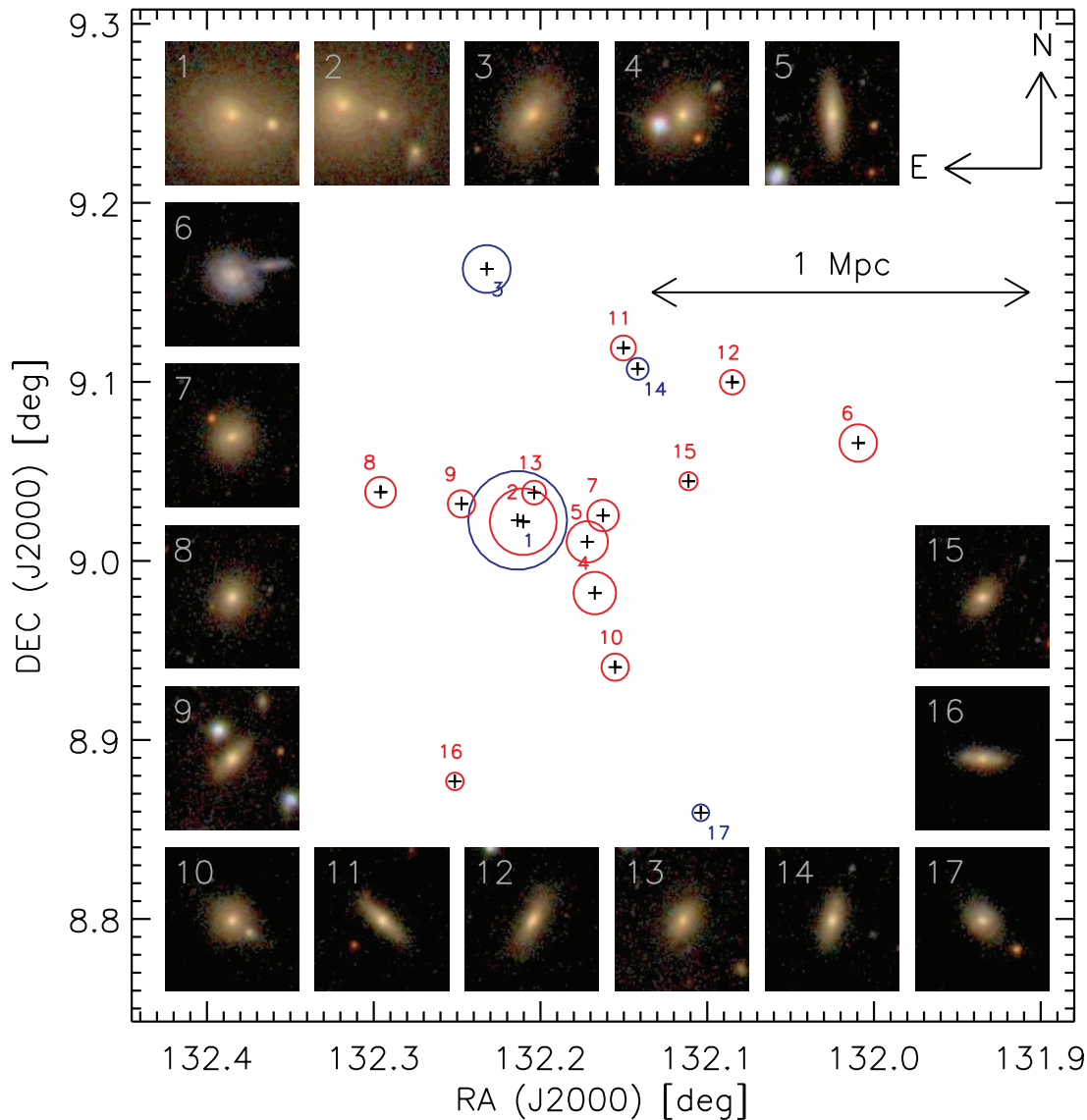


FIG. 5.—Sample rich cluster that is newly found in our study. The density ranking is 142nd of 933, with the density parameter  $\rho = 9.1$  and  $N_{\text{gal}} = 16$  within 1 Mpc, where its virial radius  $R_{200}$  is estimated to be 0.737 Mpc and  $N_{200} = 11$ . The size of each circle denotes its  $r$ -band luminosity. Blue and red circles show photometric and spectroscopic members, respectively. SDSS image cutouts are shown for the 16 members and the central MDG (No. 7). The BCG is marked as No. 1.

to  $200 \text{ km s}^{-1}$ . Among them, 212 clusters are newly found in this study.

Figure 5 shows a sample from the newly found clusters. The BCG and MDG are marked as Nos. 1 and 7, respectively. Blue and red circles denote photometric and spectroscopic members, respectively, while the size of circles is proportional to the galaxy  $r$ -band brightness. Postage images of the member galaxies are also shown. Its MDG is ranked 142nd out of 924, with  $\rho = 9.1$  and  $N_{\text{gal}} = 16$  within 1 Mpc. For comparison, the central galaxy in the Virgo Cluster, M87, has  $\rho = 7.5$  and  $N_{\text{gal}} = 19$  within 1 Mpc and thus is comparable.

Table 1 provides various properties of our galaxy clusters. The positions of MDGs and BCGs are included. The redshift of each cluster is obtained by finding the redshift peak of the spectroscopic members and fitting it by Gaussian function. When the number of spectroscopic members is less than 4, we simply find the median redshift of spectroscopic member galaxies. We calculate the virial radius  $r_{200}$  by counting the number density of

member galaxies and comparing it to the cosmological background number density of galaxies. We estimate the number of galaxies within a virial radius  $N_{200}$  by counting the galaxies within  $r_{200}$ . The velocity dispersion is calculated with a biweight estimator (Beers et al. 1990) in  $r_{200}$  after  $3\sigma$  clipping. As a proxy to the cluster size and density, we can use  $\rho$  regardless of the cluster size (virial radius).

In § 3.5 we introduced the separation between the MDGs and BCGs as a test of how well the cluster search scheme finds cluster centers. In Figure 6 we show the separation between MDGs and BCGs in our method with (*bottom*) and without (*top*) added photometric members. It illustrates the effectiveness of the added photometric members.

The galaxy number density profile is a good proxy for the mass profile and thus dark matter profile of galaxy clusters (Carlberg et al. 1997; van der Marel et al. 2000; Katgert et al. 2004; Lin et al. 2004; Hansen et al. 2005). In Figure 7, we show the galaxy number density profile of two examples. We compare them with the

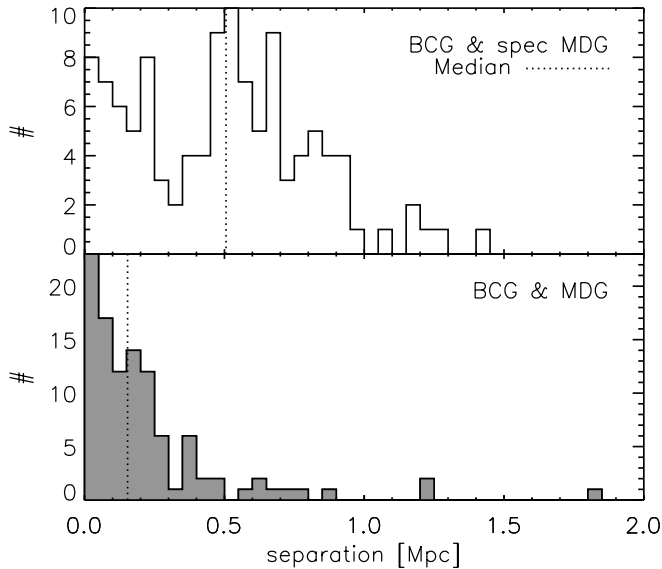


FIG. 6.—Separation between BCGs and MDGs. The dotted lines represent the median separation. The top panel shows the separation when the CMR-selected photometric members are not included in the density measurement. When we add the photometric members (*bottom*), the separation gets much smaller, yielding a more reliable cluster center detection.

Navarro-Frenk-White (NFW) dark matter profile (Navarro et al. 1996), which is defined as

$$\frac{\rho(r)}{\rho_c} = \frac{\delta_c}{(r/r_s)(1+r/r_s)^2} \quad (9)$$

and can be projected into a two-dimensional space as

$$\frac{\rho(r_p)}{\rho_c} = 2n_0 \int_0^\theta \frac{\delta_c}{(r_p/r_s \cos \theta)(1+r_p/r_s \cos \theta)^2} d\theta, \quad (10)$$

where  $n_0$  is normalization factor,  $r_p$  is projected distance, and  $\theta = \cos^{-1}(r_p/r_{200})$ . The number density profile is in reasonable agreement with the NFW profile as found also by Hansen et al. (2005). The galaxy number density profile only based on the spectroscopic members is lower than the one with photometric members added. The departure gets larger in the central region of the clusters where the spectroscopic coverage is poor.

A larger cluster would have a higher value of  $\rho$ , the density measure within 1 Mpc. We show the distribution of  $\rho$ ,  $N_{200}$ , and the velocity dispersion of clusters within  $r_{200}$  in Figure 8. The (minimum, median, maximum) for the four panels are (0, 5, 190) for  $N_{200}$ , (4.0, 5.7, 32.2) for  $\rho$ , and (0, 263, 1299) for  $\sigma$ , and the redshift range is 0.05–0.1. The density and the velocity dispersion of M87 (Binggeli et al. 1987) in the Virgo Cluster is shown as well.

In Figure 9 we compare  $\rho$  with  $N_{200}$ . Also shown is the linear fit to the data. The density parameter  $\rho$  appears to scale as a power law with  $N_{200}$  rather than with a linear relation. That is, in dense regions, the linear fit would have a steeper slope. This is because the Gaussian weight in our density measuring scheme takes the distance to each member into account. For a given number of cluster members, a more concentrated cluster would have a higher value of  $\rho$ .

In Figure 10 we compare between various cluster properties. The density parameter is a good proxy to the size of galaxy clusters. It also shows a good correlation with the velocity disper-

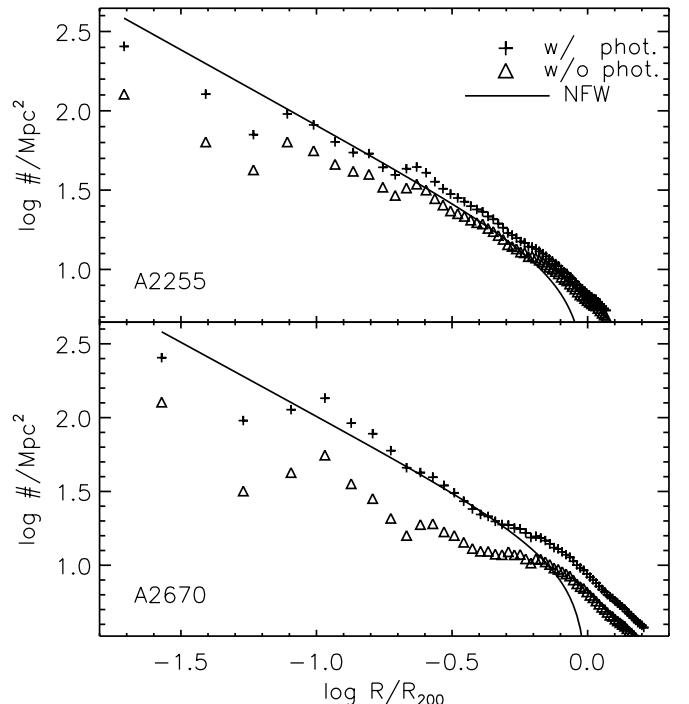


FIG. 7.—Projected radial profiles of the galaxy number density of sample rich clusters centered at their BCGs. The plus signs show the galaxy number density profiles from our scheme (including both spectroscopic and photometric members), and the triangles those with only spectroscopic members. Also shown for comparison are the projected NFW halo profiles fitted to our measurements *with* both spectroscopic and photometric members. Our measurements are in good agreement with the projected NFW profiles.

sion of clusters. Thus, our density parameter can be an obvious indicator of dynamical mass of a galaxy cluster as well, as shown in the bottom panel.

#### 4.2. Comparison to Other Catalogs

We perform a cross-matching between existing catalogs and ours. The matching criteria are 2 Mpc in the projected radius and  $\Delta z = 0.01$ . When the known clusters do not have redshift (e.g., Zwicky clusters), we just match them within 2 Mpc radius in the sky. Each cluster in our catalog is matched with other catalogs separately. The clusters that are detected in our method are generally in the existing catalogs (see Table 2). Most rich clusters are matched with Abell or Zwicky clusters, and this implies that the new algorithm using MDGs successfully finds rich galaxy clusters. For those clusters in the existing catalogs that include redshift, we can check the rate at which our method recovers clusters known previously. Some Abell clusters have redshifts, and the C4 catalog clusters always do (Miller et al. 2005). We cross-check our clusters against the Abell and C4 clusters that are in the SDSS area and in our redshift range. In our method 128 of 162 Abell clusters with redshifts and 300 of 458 C4 clusters are detected, corresponding to detection rates of 79% and 66%, respectively. If we lowered the  $\rho$  cut for “clusters” from 4.0 to 1.0 we would find 89% and 95% of Abell and C4 clusters, respectively. For example, by using a  $\rho = 1$  cut, we can recover 18 additional Abell clusters. However, such a low value of cut ( $\rho \sim 1.0$ ) would also find significantly more cluster candidates (3959), many of which may be false detections. Our density measures with  $\rho = 4$  cut are in general based on about seven member galaxies. Besides, when only a small number of galaxies are used for density measurement, the density measures become less reliable, too. Since

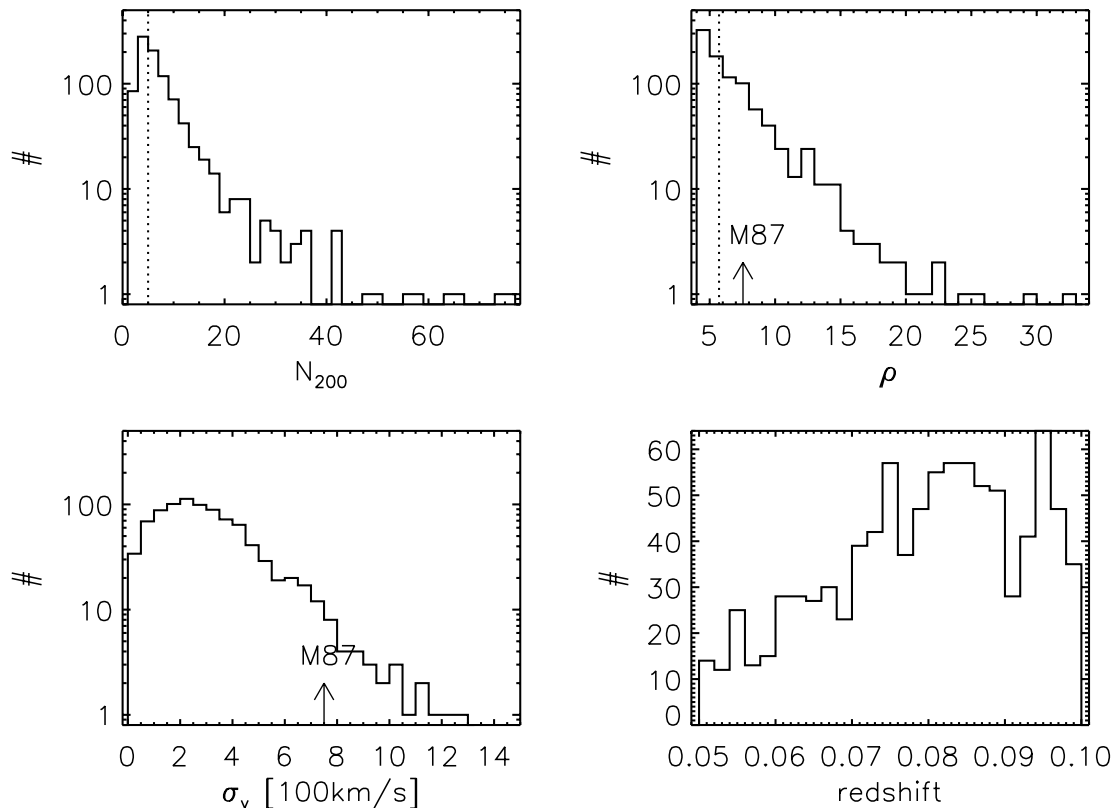


FIG. 8.—Histogram of  $N_{200}$ ,  $\rho$ , velocity dispersion, and redshift. We define galaxy clusters when a condition  $\rho \geq 4.0$  is met. In the top left panel two clusters of  $N_{200} = 190$  and  $148$  are out of bounds. The vertical dotted lines show median values. The density and velocity dispersion of M87 are shown as the arrow.

our goal is to construct a database of galaxy clusters with *improved* and hence reliable density measures, we think our  $\rho = 4.0$  cut is a good compromise. However, we admit that this choice is still somewhat arbitrary and by using this cut we are neglecting smaller clusters. In this regard, our 924 cluster candidates represent a robust sample of relatively rich clusters.

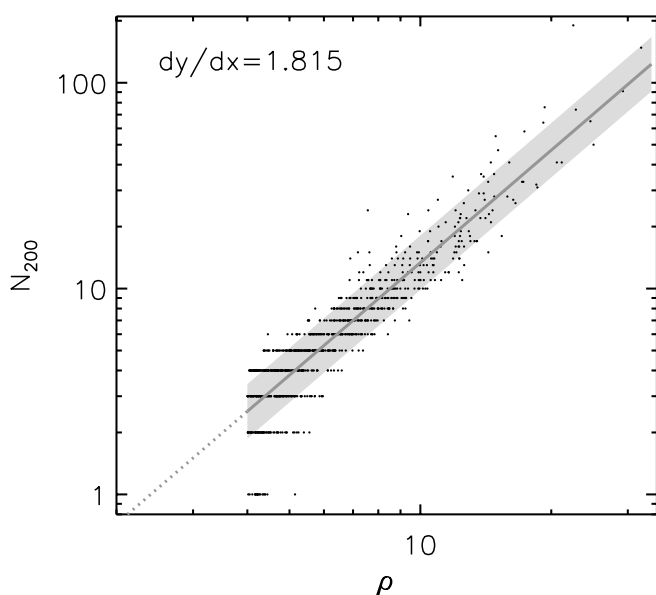


FIG. 9.—Density parameter  $\rho$  is proportional to  $N_{200}$  scaling as power law. Note that the density parameter includes the distance information in addition to the number. The thick line shows the linear fit to the data, and the gray band shows the standard error of the fit.

The galaxy clusters that were known to Abell but missed by our method are mostly due to the  $\rho$  cut as mentioned above. In addition, our method missed nine Abell clusters that are mainly composed of relatively faint galaxies that do not make it to our volume-limited sample. Two Abell clusters were missed because they are found by our method to be parts of larger clusters, just like the M87 and M49 groups in the Virgo Cluster. Five additional clusters were missed due to various minor reasons: e.g., mismatch in the redshift of the center galaxy of a cluster, mismatch in the position of the center galaxy of a cluster, and so on.

We compare our new catalog to the C4 cluster catalog (Miller et al. 2005). While we use the density  $\rho$  to represent the richness of a cluster, the C4 catalog provides the number of galaxies within various radii. We compare our density measures within 1 Mpc,  $\rho$ , with the C4 richness (C4 parameter  $w_{\text{mag}1000}$ ) in Figure 11. The match is reasonably good but shows a large scatter. The systematic difference in vertical scale has a couple of critical origins. Most importantly, our limiting magnitude,  $M_r = -20.5$ , is somewhat brighter than that of C4 ( $-19.9$ ). Second, our density is not a simple count of galaxies but weighted by the distance from the cluster center. Third, our method, unlike C4, includes additional photometric member candidates. Fourth, our choice for the search radius (1 Mpc) is smaller than that of C4 ( $1 h^{-1}$  Mpc). Last, the member search volume in C4 is a cylinder with a line-of-sight length corresponding to 4 times the velocity dispersion, while ours is an ellipsoid with a length that is 3 times the velocity dispersion. The large scatter is mainly a result of two effects. To begin with, the position of the central galaxy of a cluster can be different mainly because our method includes photometric member candidates. In addition, the redshift of a cluster can also be different. We notice some difference in the velocity dispersion measured as well, which also contributes to the scatter.

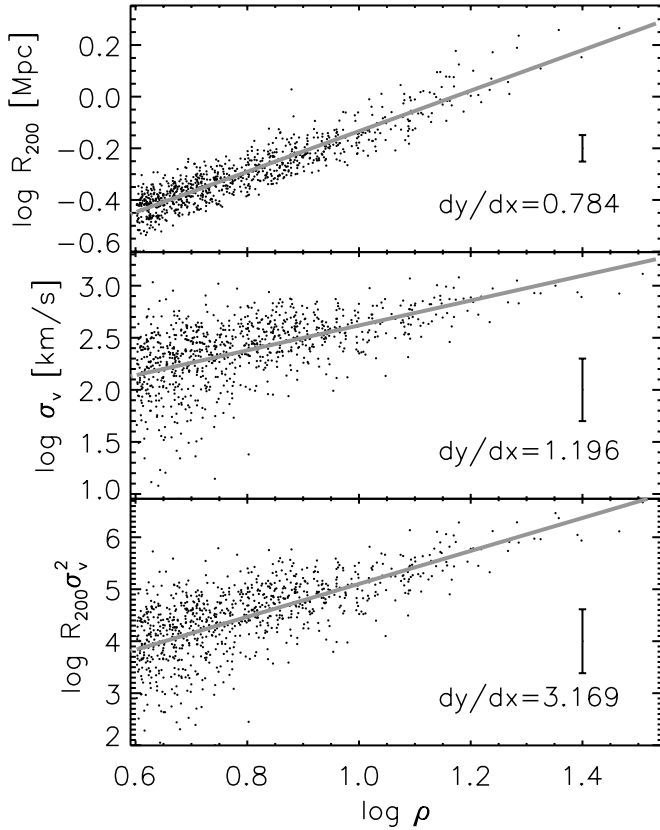


FIG. 10.—Density parameter  $\rho$  is in agreement with the properties representing the mass and size of clusters. The virial radius in the top panels has a tight correlation with  $\rho$ . The density parameter correlates with the velocity dispersion and dynamical mass in the middle and bottom panels. The thick gray line shows our linear fit, and  $dy/dx$  presents the exponents of the power law. The error bars represent mean scatter.

4.3. Effects of Photometric Members

The inclusion of the CMR-selected photometric members increases our local density measures by  $\sim 22\%$  (see Fig. 12). In this figure, the small black dots show the density measures of our clusters based only on the SDSS database. A linear fit to the data is shown as a dashed line (showing the 22% increase), and the one-to-one relation is presented as a dotted line.

To check the validity of the CMR technique further, we attempt to recover our spectrophotometric density *approximately* by dividing the measured spectroscopic density  $\rho_{\text{spec}}$  by the estimated spectroscopic completeness fraction  $f_{\text{spec}}$ . Figure 13 compares  $\rho_{\text{spec}}/f_{\text{spec}}$  (*crosses*) with our spectrophotometric density  $\rho$  (*upper*

TABLE 2  
THE NUMBER OF GALAXY CLUSTERS FOUND  
IN OUR SCHEME MATCHED TO PREVIOUS CATALOGS

Cluster Catalog	Number	Recovery (%)
Abell.....	128	79
Zwicky .....	457	...
C4.....	300	66
Others.....	889	...
Newly found.....	212	...
Total.....	924	

NOTE.—The existing cluster catalogs are from the VizieR Catalogue Service.

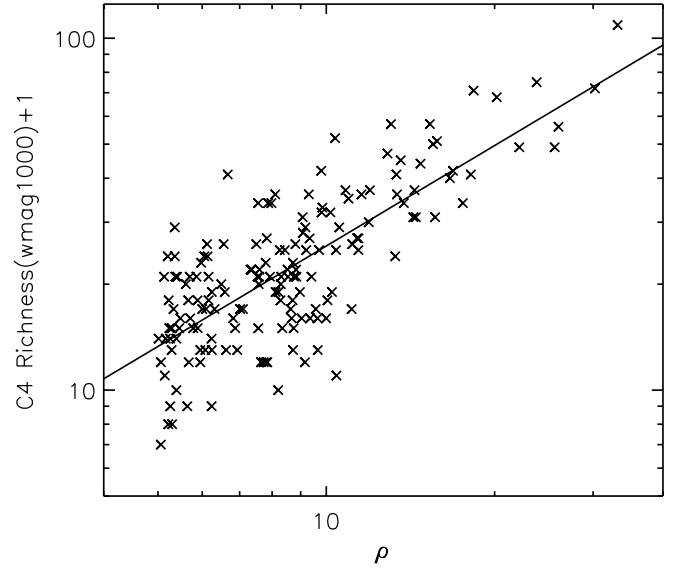


FIG. 11.—Comparison between catalogs in terms of the richness of the clusters. The x-axis shows our density parameter  $\rho$  (listed in Table 1), and the y-axis shows  $N_{\text{gal}}$  (wmag1000) from the C4 catalog. The large scatter has several origins (see text for details). The line shows the linear fit.

*ends of arrows*). They agree reasonably well. Since  $\rho$  is a complex parameter including the distance information while  $f_{\text{spec}}$  is not, we also make the comparison to  $N_{\text{gal}}$ , which also shows a tight correspondence.

4.4. Additional Spectroscopy for the Test

For 22 of our clusters we were able to find 2dF spectroscopic data with which we identified further member galaxies. Using these new spectroscopic members, we computed new (enhanced)  $\rho_{\text{spec}}$  and compared them to our SDSS-spectrophotometric  $\rho$  in

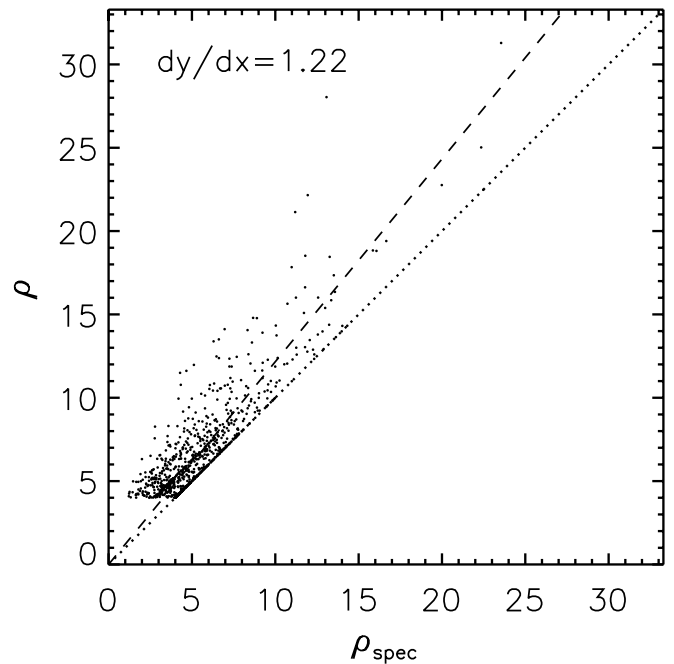


FIG. 12.—We compare our density measure  $\rho$  with  $\rho_{\text{spec}}$  (the density only with spectroscopic data). The dotted line presents the one-to-one relation between  $\rho$  and  $\rho_{\text{spec}}$ , and the dashed line shows a linear fit with the y-intercept fixed at the origin. The departure gets larger in dense regions. The density increases by 22% through the addition of photometric member galaxies.

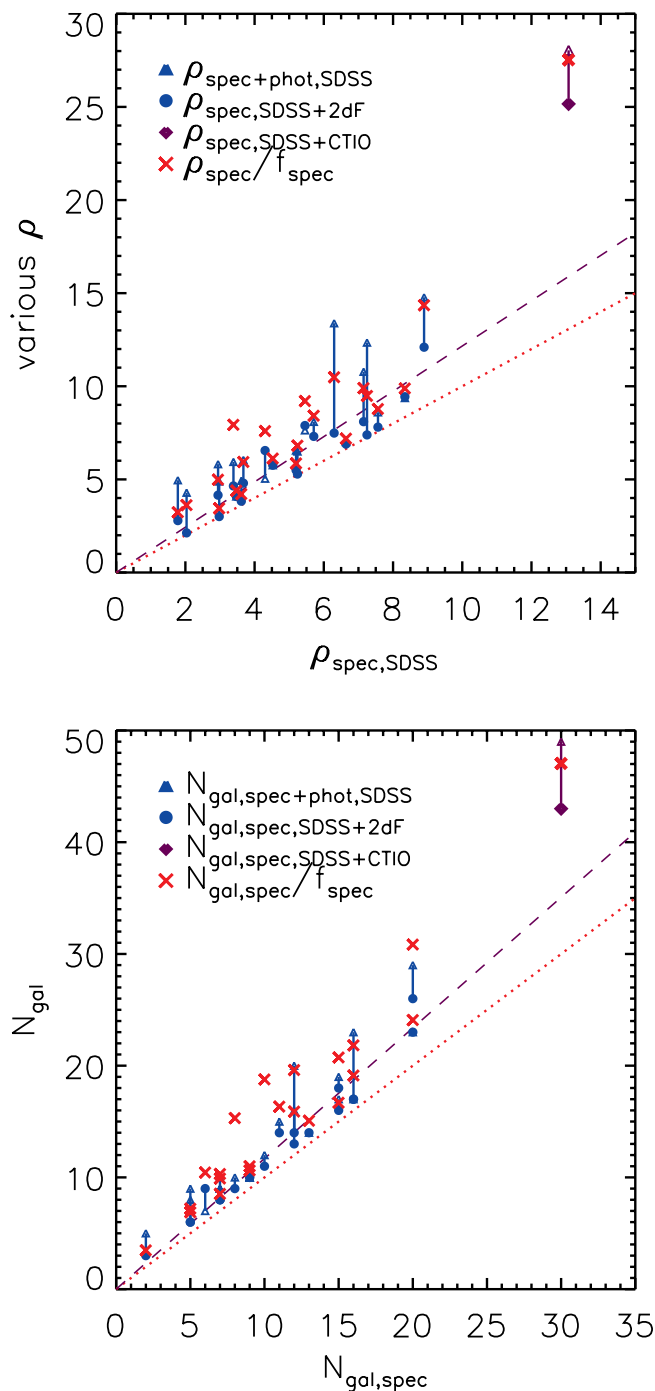


FIG. 13.—*Top*: Comparison between the spectroscopy-only density measures ( $x$ -axis) and various improved density measures ( $y$ -axis). The filled triangles show our spectrophotometric densities ( $\rho$ ). The filled circles show the spectroscopic densities based on the SDSS and 2dF database combined. The purple diamond in the top right shows the spectroscopic density of Abell 2670 based on both the SDSS and our new CTIO database. The crosses show the result of rough correction for the incompleteness problem, using  $\rho_{\text{spec}}$  (i.e.,  $x$ -axis) and the completeness fraction  $f_{\text{spec}}$ . *Bottom*: Same as the top panel but for the number of galaxies. The dotted and dashed lines are the same as in Fig. 12.

Figure 13. The  $x$ -axis shows our 2D SDSS-spectroscopic density ( $\rho_{\text{spec}}$ ) that suffers from the incompleteness problem. The  $y$ -axis shows density measures improved on  $\rho_{\text{spec}}$  through various methods. The blue filled circles show the new spectroscopic density measures for the 22 clusters including the added 2dF member candidates:  $\rho_{\text{spec,SDSS+2dF}}$ . Only a few of the new SDSS+2dF

spectroscopic density measures ( $\rho_{\text{spec,SDSS+2dF}}$ ) overshoot our 22% enhancement prediction (*dashed line*). Even in this case, however, the SDSS+2dF spectroscopic density measures ( $\rho_{\text{spec,SDSS+2dF}}$ ) are still lower than our SDSS-only spectrophotometric density measures ( $\rho_{\text{spec+phot,SDSS}}$ ; that is, our density measures in eq. [6]) in most cases, as indicated by the arrows. The end points of the arrows indicate our SDSS-spectrophotometric density measures.

In order to test our result, we have performed Cerro Tololo Inter-American Observatory (CTIO) Hydra MOS observation of Abell 2670 and significantly increased the spectroscopic coverage of this cluster from 65% (within 1 Mpc) to 92%. We chose this cluster as a test case because it suffers from an extreme case of the spectroscopic incompleteness problem as mentioned in § 1.

The observation was performed on 2006 December 1–3 with Hydra, a multi-object spectrograph mounted on the Blanco 4 m Telescope at CTIO. The wavelength range covers 3600–8000 Å, and the spectral resolution is 2.3 Å pixel<sup>-1</sup> with mean signal-to-noise ratio of 13. Originally all of the early-type galaxies in Abell 2670 with  $r < 18$  were selected as targets. In order to execute our plan as completely as possible, we used three fiber configurations to evade fiber collision issues in dense regions. For each fiber configuration, a total of 45 minutes, which consists of three exposures of 15 minutes, was taken for median combine and cosmic-ray removal. All the processes were done mainly with the IRAF hydra package. The radial velocities of galaxies were measured by the cross-correlation method using the IRAF rvsao package and cross-correlation templates of SDSS. In the top right of Figure 13, we show our new SDSS+CTIO spectroscopic density ( $\rho_{\text{spec,SDSS+CTIO}}$ ) at  $\approx 25$  (*purple diamond at top right*). The value, based on a relatively complete (92%) spectroscopic survey, now is a factor of 2 larger than the previous  $\rho_{\text{spec,SDSS}}$  and much closer to our spectrophotometric density  $\rho_{\text{spec+phot,SDSS}}$ . This validates our spectrophotometric density measurement scheme.

## 5. SUMMARY

We develop and test a method for finding galaxy clusters in the SDSS spectroscopic and photometric database. Our method is an improvement over the previous density measurements by finding an additional cluster member candidates via the color-magnitude relation technique. The problem of spectroscopic incompleteness due to fiber collisions in dense fields is minimized in our method. The member galaxies selected by the color-magnitude relation lead to a satisfactory completeness and purity. With this method, we find 924 galaxy clusters of which 212 are new. We provide a catalog of these clusters including important properties such as the virial radius, velocity dispersion, and richness parameters. The density that we estimate is in good agreement with the properties relating to the cluster mass and size. We also provide an estimating scheme for our spectrophotometric density measure simply using the spectroscopic completeness rate. Our new density information on galaxy clusters could be useful for the study of the environmental effect on galaxy evolution.

We thank the anonymous referee for numerous suggestions and criticisms that improved the clarity of the paper. We would like to thank Jong-Hak Woo and Sangmo Sohn for their help in the data reduction. This work was supported by grant No. R01-2006-000-10716-0 from the Basic Research Program of the Korea Science and Engineering Foundation to the corresponding author S. K. Y.

## REFERENCES

- Abadi, M. G., Moore, B., & Bower, R. G. 1999, *MNRAS*, 308, 947
- Abell, G. O. 1958, *ApJS*, 3, 211
- Abell, G. O., Corwin, H. G., & Olowin, R. P. 1989, *ApJS*, 70, 1
- Bahcall, N. A., et al. 2003, *ApJS*, 148, 243
- Balogh, M., et al. 2004a, *MNRAS*, 348, 1355
- Balogh, M. L., Baldry, I. K., Nichol, R., Miller, C., Bower, R., & Glazebrook, K. 2004b, *ApJ*, 615, L101
- Baum, W. A. 1959, *PASP*, 71, 106
- Beers, T. C., Flynn, K., & Gebhardt, K. 1990, *AJ*, 100, 32
- Bekki, K. 1999, *ApJ*, 510, L15
- Binggeli, B., Tammann, G. A., & Sandage, A. 1987, *AJ*, 94, 251
- Blanton, M. R., Eisenstein, D., Hogg, D. W., Schlegel, D. J., & Brinkmann, J. 2005, *ApJ*, 629, 143
- Blanton, M. R., et al. 2003a, *AJ*, 125, 2276
- . 2003b, *AJ*, 125, 2348
- Boselli, A., & Gavazzi, G. 2006, *PASP*, 118, 517
- Byrd, G., & Valtonen, M. 1990, *ApJ*, 350, 89
- Capak, P., et al. 2007, *ApJS*, 172, 284
- Carlberg, R. G., et al. 1997, *ApJ*, 485, L13
- Christlein, D., & Zabludoff, A. I. 2005, *ApJ*, 621, 201
- Chung, A., van Gorkom, J. H., Kenney, J. D. P., & Vollmer, B. 2007, *ApJ*, 659, L115
- Colless, M., et al. 2001, *MNRAS*, 328, 1039
- Croft, R. A. C., Dalton, G. B., Efstathiou, G., Sutherland, W. J., & Maddox, S. J. 1997, *MNRAS*, 291, 305
- Croton, D. J., et al. 2005, *MNRAS*, 356, 1155
- Dalton, G. B., Efstathiou, G., Maddox, S. J., & Sutherland, W. J. 1994, *MNRAS*, 269, 151
- Dressler, A. 1980, *ApJ*, 236, 351
- Dressler, A., et al. 1997, *ApJ*, 490, 577
- Elbaz, D., et al. 2007, *A&A*, 468, 33
- Farouki, R., & Shapiro, S. L. 1980, *ApJ*, 241, 928
- Fujita, Y., & Nagashima, M. 1999, *ApJ*, 516, 619
- Giovanelli, R. G., Haynes, M. P., & Chincarini, G. L. 1986, *ApJ*, 300, 77
- Gisler, G. R. 1978, *MNRAS*, 183, 633
- Gladders, M. D., & Yee, H. K. C. 2000, *AJ*, 120, 2148
- Gomez, P. L., et al. 2003, *ApJ*, 584, 210
- Goto, T., et al. 2003, *MNRAS*, 346, 601
- Gunn, J. E., & Gott, J. R. 1972, *ApJ*, 176, 1
- Hansen, S. M., McKay, T. A., Wechsler, R. H., Annis, F., Sheldon, E. S., & Kimball, A. 2005, *ApJ*, 633, 122
- Hogg, D. W., et al. 2004, *ApJ*, 601, L29
- Katgert, P., Biviano, A., & Mazure, A. 2004, *ApJ*, 600, 657
- Kim, R. S. J., et al. 2002, *AJ*, 123, 20
- Kochanek, C. S., et al. 2003, *ApJ*, 585, 161
- Larson, R. B., & Tinsley, B. M. 1978, *ApJ*, 219, 46
- Larson, R. B., Tinsley, B. M., & Caldwell, C. N. 1980, *ApJ*, 237, 692
- Lewis, I., et al. 2002, *MNRAS*, 334, 673
- Lin, Y.-T., Mohr, J. J., & Stanford, S. A. 2004, *ApJ*, 610, 745
- López-Cruz, O., Barkhouse, W. A., & Yee, H. K. C. 2004, *ApJ*, 614, 679
- Lumsden, S. L., Nichol, R. C., Collins, C. A., & Guzzo, L. 1992, *MNRAS*, 258, 1
- Makino, J., & Hut, P. 1997, *ApJ*, 481, 83
- Matthews, T. A., Morgan, W. W., & Schmidt, M. 1964, *ApJ*, 140, 35
- Miller, C. J., et al. 2005, *AJ*, 130, 968
- Moore, B., Katz, N., Lake, G., Dressler, A., & Oemler, A. 1996, *Nature*, 379, 613
- Moore, B., Lake, G., Quinn, T., & Stadel, J. 1999, *MNRAS*, 304, 465
- Navarro, J. F., Frenk, C. S., & White, S. D. M. 1996, *ApJ*, 462, 563
- Oegerle, W. R., & Hill, J. M. 2001, *AJ*, 122, 2858
- Park, C., Choi, Y.-Y., Vogeley, M. S., Gott, J. R., & Blanton, M. R. 2007, *ApJ*, 658, 898
- Postman, M., & Geller, M. J. 1984, *ApJ*, 281, 95
- Postman, M., et al. 1996, *AJ*, 111, 615
- . 2005, *ApJ*, 623, 721
- Quilis, V., Moore, B., & Bower, R. 2000, *Science*, 288, 1617
- Quintero, A. D., Berlind, A. A., Blanton, M. R., & Hogg, D. W. 2006, *ApJ*, submitted (astro-ph/0611361)
- Schawinski, K., et al. 2007, *ApJS*, 173, 512 (S07)
- Schlegel, D. J., Finkbeiner, D. P., & Davis, M. 1998, *ApJ*, 500, 525
- Shectman, S. A. 1985, *ApJS*, 57, 77
- Stoughton, C., et al. 2002, *AJ*, 123, 485
- Strauss, M. A., et al. 2002, *AJ*, 124, 1810
- Thomas, D., Maraston, C., & Bender, R. 2005, *ApJ*, 621, 673
- Toomre, A., & Toomre, J. 1972, *ApJ*, 178, 623
- Tully, R. B. 1988, *AJ*, 96, 73
- Valluri, M. 1993, *ApJ*, 408, 57
- van der Marel, R. P., Magorrian, J., Carlberg, R. G., Yee, H. K. C., & Ellingson, E. 2000, *AJ*, 119, 2038
- Visvanathan, N., & Sandage, A. 1977, *ApJ*, 216, 214
- von der Linden, A., Best, P. N., Kauffmann, G., & White, S. D. M. 2007, *MNRAS*, 379, 867
- Whitmore, B. C., & Gilmore, D. M. 1991, *ApJ*, 367, 64
- York, D. G., et al. 2000, *AJ*, 120, 1579
- Zwicky, F., Herzog, E., Wild, P., Karpowicz, M., & Kowal, C. 1961–1968, *Catalog of Galaxies and Clusters of Galaxies*, Vols. 1–6 (Pasadena: Caltech)